

Research on Engineering Structures & Materials



www.jresm.org

Research Article

Comparative analysis of inelastic behavior of RC beam using applied element method and finite element method

Hasibullah Azizi*, a, SK. Yajdani b

Department of Civil Engineering, Andhra University, India

Article Info

Abstract

Article History:

Received 17 May 2025 Accepted 21 Oct 2025

Keywords:

Inelastic behavior; Cracking patterns; Applied element method: Finite element method

Investigating the inelastic behavior of entire buildings and their structural elements under hazard-induced forces is crucial. The Applied Element Method (AEM) is a simulation-based analysis technique capable of modeling performance from initial loading to eventual failure. This paper presents a comparative analysis of AEM and the Finite Element Method (FEM) in simulating the inelastic performance of a reinforced concrete beam, with results validated against experimental data. The structural analysis was performed using two different numerical methods: The AEM, implemented in the Extreme Loading for Structures (ELS) software, and the FEM, implemented in ABAQUS. The comparison showed that both numerical models closely matched the observed overall structural response, especially in the elastic phase. Additionally, both methods accurately captured the failure mode, load-deflection behavior, and crack pattern development under 6 % error, based on the experimental data. While both methods reasonably predicted the elastic moment, FEM estimated a higher plastic moment capacity. The findings indicate that both AEM and FEM are effective in tracking the linear and nonlinear inelastic performance of the RC beams, supporting safe, durable, and cost-effective building designs.

© 2025 MIM Research Group. All rights reserved.

1. Introduction

Understanding the inelastic performance of critical structural elements, such as reinforced concrete beams, during seismic incidents remains a key concern in structural engineering. The Türkiye-Syria earthquake, which occurred on February 6, 2023, with an initial seismic intensity of 7.8, was followed nine hours later by a 7.5-magnitude aftershock. This unintentional event resulted in approximately 50,000 deaths. This widespread devastation also resulted in the collapse of 37,066 buildings and critical damage to over 200,000 structures [1]. The destructive structural failures observed during the 2023 Türkiye-Syria earthquake highlighted the limitations of conventional numerical techniques in predicting progressive collapse and inelastic performance. In light of this, advanced numerical methods such as the AEM and FEM offer superior functionality for capturing crack propagation and failure mechanisms in reinforced concrete structures, making them well-suited for understanding failure mechanisms observed in events like the Türkiye-Syria earthquake.

The AEM and FEM can be utilized to develop effective numerical methods for simulating the performance of individual structural elements under various loading conditions, thus providing an accurate representation of both elastic and inelastic behavior. AEM's ability to simulate the performance of specific structural elements, like beams under different types of loads, including seismic forces, offers valuable insights into failure mechanisms and overall structural strength [2-4].

*Corresponding author: hasibullah3g@gmail.com

^aorcid.org/0000-0001-9762-9670; ^borcid.org/0009-0002-6471-8866

DOI: http://dx.doi.org/10.17515/resm2025-907st0517rs

Res. Eng. Struct. Mat. Vol. x Iss. x (xxxx) xx-xx

In AEM, the structure is idealized as an assembly of individual components, created by virtually separating the structural elements. These components are connected by two pairs of springs, which provide counterforce in both orthogonal and transverse directions [2]. This type of interface allows components to separate independently and enables the modeling of cracks and plastic hinges. Conversely, the Finite Element Method (FEM), a traditional computational analysis approach, does not automatically model component separation unless the locations of plastic hinges and cracks are predefined [3]. Furthermore, FEM, based on continuum material techniques, makes it difficult to capture the progressive failure of components, highlighting a limitation of this approach [4].

In contrast, AEM combines the advantages of continuum and Discrete Element Method (DEM) approaches, allowing it to serve as a reliable, faster, and easier computational tool for element simulation. This advantage makes AEM more effective than other methods in designing safe, durable, and cost-efficient buildings [5]. The AEM has proven to be a powerful numerical method that bridges the gap between FEM and DEM, offering the capability to simulate both continuum and discrete behavior of structures. It has shown significant potential in analyzing various structural behaviors, including cracking, crushing, separation, and failure. Developed by Meguro and Tagel-Din [3], this numerical method is especially effective for simulating the progressive collapse of structures because it can automatically detect element separation without requiring remeshing.

In recent years, various studies have validated the accuracy and applicability of AEM across a wide range of structural applications. For example, Meguro and Tagel-Din [4] applied AEM to analyze the seismic performance of reinforced concrete (RC) frames and illustrated its superior ability to predict progressive failure. This was further supported by the successful study of AEM in modeling the complete failure of a three-dimensional RC frame structure under seismic loading [6]. Other researchers, Kalliontzis and Stylianidis [7] applied the AEM to investigate the collapse behavior of precast RC frame structures, demonstrating its capability to realistically model progressive failure sequences and present sudden changes in structural integrity. In a related investigation, Botez, Bredean, and Ioani assessed the potential of the AEM for evaluating the progressive collapse of low-rise reinforced concrete framed structures, highlighting its capability to represent discontinuities and sudden changes in structural integrity better than traditional FEM methods [8].

The merit of AEM lies in its unique element formulation. Structures are discretized into rigid elements integrated by normal and shear springs that model material behavior at the interface level [9]. These springs can represent elastic and inelastic behaviors, as well as fracture and separation of elements, making AEM well-suited for progressive collapse and failure modeling scenarios. Unlike FEM, AEM does not require shape functions or numerical integration to formulate global stiffness matrices, thereby simplifying the computational process and enhancing efficiency [10]. The implementation of AEM is not limited to RC and masonry structures. It has also been used to simulate steel frames, bridges, and even historical heritage buildings, where accurate simulation of cracking and failure is crucial.

Despite its advantages, AEM has its limitations. The numerical method can become computationally intensive for large-scale 3D models, and its accuracy heavily depends on mesh size and spring stiffness formulation [11]. Despite this, further advancement and integration with commercial software like Extreme Loading for Structures (ELS) have made AEM increasingly accessible for practical engineering applications. In essence, the AEM has proven to be a reliable and innovative tool for simulating structural performance under extreme conditions. With its capacity for modeling crack initiation, propagation, and structural failure, AEM continues to gain traction as a reliable alternative to conventional numerical methods in structural analysis [4]. The FEM has long been the foundation of computational structural mechanics for decades, supported by extensive research and development. Its reliability in modeling material nonlinearity, complex boundary conditions, and the pre-failure response of structures is well documented in influential literature [13-17]. As a mature and widely validated technique, FEM serves as a key benchmark for evaluating the performance of new numerical approaches.

A key challenge, however, lies in simulating a structure's complete lifecycle, from initial loading to ultimate collapse and disintegration. While FEM is highly reliable for pre-peak behavior, its accuracy can diminish in the post-failure phase due to challenges associated with extensive element

distortion and deletion. In contrast, the AEM is specifically designed to maintain accuracy even during large displacements and structural separation. The overview of the prevailing literature is summarized in Table 1, which rates the method's ability on a scale from excellent, good, to limited based on structural behavior from initial loading to complete collapse [2-11].

Table 1. Structur	al behavior fron	n initial loading to	complete collapse
I abic II bu accai	ar bellavior iron	ii iiiiiciai ioaaiiig co	complete comapse

Analysis Phase / Method	Finite Element Method (FEM)	Discrete Element Method (DEM)	Applied Element Method (AEM)
Linear Elastic Analysis	Excellent	Not Primary Use	Excellent
Linear Elastic Allalysis	Excenent	Not Filliary Use	Excellent
Non-Linear Material	Good	Limited	Good
Behavior	(Requires user-defined	(Challenging for	(Automated through
(Cracking, Yielding,	constitutive models)	concrete continuum)	spring failure)
Crushing)			
Geometric Instability	Good	Not Primary Use	Good
(Buckling, Post-	(Requires specialized		(Captured through
Buckling)	analysis steps)		element instability)
Structural Separation	Limited	Inherent Capability	Inherent Capability
& Collapse	(Challenged by element	(Designed for discrete	(Core strength;
(Element Separation,	distortion/deletion)	bodies)	automated
Debris Formation)			separation)
Post-Collapse	Very Limited	Excellent	Good
Behavior	(Not designed for debris	(Explicitly simulates	(Models rigid body
(Rigid Body Motion,	contact)	collisions)	motion & contact)
Collision)			

As the comparative summary illustrates, no single method is universally better; rather, their efficacy is highly dependent on the analytical objective. The FEM demonstrates strong capabilities for predicting serviceability and initial inelasticity, providing detailed stress distributions within the continuum. Conversely, the AEM is specifically designed to excel in the post-failure regime, automatically capturing the progression of collapse through element separation. Therefore, choosing between FEM and AEM depends on the specific phase of structural behavior being studied. FEM is typically preferred for pre-failure analysis, while AEM has a clear advantage in collapse simulation. This study provides a comparative evaluation of the AEM and FEM for simulating the inelastic behavior of an RC beam, to highlight the strengths and limitations of each method.

The paper is organized into the following sections: methodology, covering experimental aspects in sections 2 and 3; the numerical modeling of FEM and AEM is demonstrated in section 4; an extensive comparison of results is outlined in section 5; and finally, conclusions are discussed in detail in section 6.

2. Methodology

The AEM is often utilized to analyze the inelastic performance of reinforced concrete (RC) beams with the assistance of the ELS (Extreme Loading for Structures, version 8.0) program [18]. This tool is designed to simulate individual members as well as complete 3D models of buildings composed of various materials, including reinforced concrete, steel, wood, and composite materials. It can model structures from the initial loading stage through to total collapse under various loading types, such as cyclic-static, cyclic-dynamic, harmonic-static, and harmonic-dynamic. Additionally, it can analyze structures under seismic loading conditions. The AEM is validated by comparing its results with those from the FEM and experimental data from the literature review [12], both of which are used to examine the accuracy of the simulation. The methodology flowchart is illustrated in Figure 1 below.

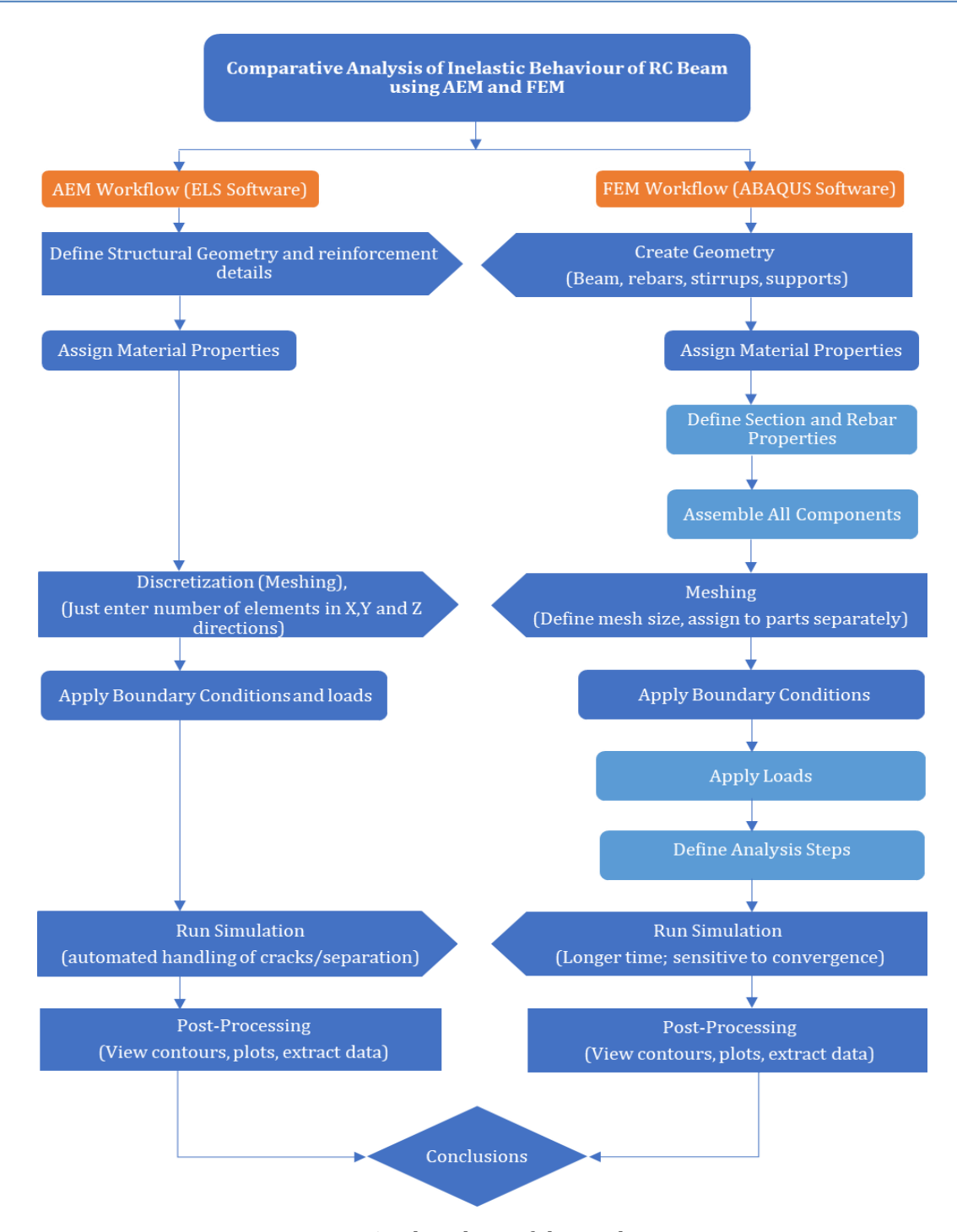


Fig. 1. Flowchart of the study

3. Experimental Setup

A reinforced concrete beam of measuring 150 mm x 250 mm x 2000 mm with a compressive strength of 25 MPa, made from conventional concrete, is considered for validation purposes as a reference study from Azeez, Mohammed Rahil, et al. [12], specimen ID (B1) was selected for validation due to its precise geometry, detailed material specifications, and availability of load deflection behavior results along with crack patterns. The beam was subjected to a gradually and linearly applied monotonic load with an interval of 5 kN until failure, configuring it for quasi-static numerical analysis using both FEM and AEM in this paper. The reinforcement used has a tensile strength of 550 N/mm 2 . The material properties and geometry of the concrete and bars are represented in Table 2 and Figure 2 [12].

Table 2. Details of Material Properties

Property	Description	Symbol	Value	Unit
Concrete				
Compressive	Maximum compressive stress in	f_c	25	MPa
Strength Modulus of	concrete			
Elasticity	Stiffness of concrete material	E_c	25000	MPa
Poisson's Ratio	Ratio of lateral strain to axial strain	ν	0.2	
Shear Modulus	Material's resistance to deformation under shear stress.	$G_{\rm c}$	10416.667	MPa
Density	Mass per unit volume of concrete	ρ	2400	Kg/m3
Reinforcing Bar				
Tensile Strength	The stress at which steel starts yielding	f_y	550	MPa
Modulus of Elasticity	Stiffness of reinforcing steel	E_{s}	2×10^{5}	MPa
Shear Modulus	Material's resistance to deformation under shear stress.	G_{s}	76923.077	MPa
Poisson's Ratio	Ratio of lateral strain to axial strain	ν	0.3	
Diameter of main	Diameter of bars in main	d	2Ø12 bottom,	mm
Bars	reinforcement	u	2Ø10 top	111111
Diameter of	Diameter of bars used for shear	d_{st}	Ø8@150mm	mm
Stirrups	reinforcement	~-3t	c/c	

The beam geometry, material properties, and reinforcement details provided in Table 2, as well as in Figure 2, were used as input parameters for both numerical models, FEM and AEM, to accurately replicate the experimental conditions. Maintaining identical properties across all models ensures a reliable comparison of the results in terms of critical load and failure mode, load deflection behavior, elastic and plastic moments, and crack patterns.

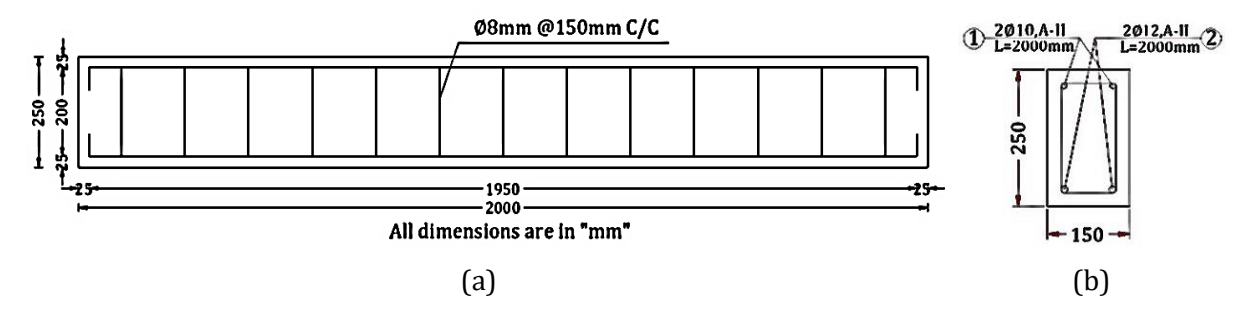


Fig. 2. Geometry of the Beam, (a) Front view, (b) Cross section

4. Numerical Modeling

4.1 Finite Element Modeling

The numerical modeling method is used to study the behavior of elements under various loading conditions. FEM has been widely validated as a dependable tool for simulating complex fracture mechanisms and structural behavior in various composite materials, including fiber-reinforced asphalt [19] and recycled aggregate concrete [20]. Experimental investigations are time-consuming, costly, and demand a large amount of materials [21]. To overcome these challenges, numerical methods such as FEM, DEM, and AEM are developed. ABAQUS/CAE 2020 software is used to analyze the beam, which is well-suited for the inelastic behavior of elements, particularly in RC elements [22]. It handles everything from basic linear analysis to complex nonlinear simulations. With its extensive library, ABAQUS can efficiently model virtually any geometry [23]. In continuation of the FEM application, the concrete beam was developed using a 3D solid mesh of

20 mm size with C3D8R elements. In contrast, the reinforcement, including both main bars and transverse reinforcement (stirrups), was modeled using embedded 2D truss elements. The boundary conditions were assigned as simply supported at both ends, and a centralized load was assigned at mid-span through a displacement-controlled loading setup. This setup was selected to simulate the experimental conditions under a quasi-static loading scenario. The analysis was conducted using the Static General step in Abaqus. The concrete damage plasticity (CDP) model was adopted for the nonlinear material behavior of concrete with standard parameter values as shown in Table 3 [24]. In the numerical analysis of the inelastic behavior of the beam, stress-strain data in both compression and tension, including yield stress, yield strain, and inelastic strain, which incorporates crack strain, are applied using Figures 3 and 5.

Table 3. Plasticity flow parameters for concrete damage plasticity

Plasticity flow characteristics						
Dilation Angle	Eccentricity	f _{bo} /f _{co}	К	Viscosity parameter		
34	0.1	1.16	0.666	0.0001		

4.1.1 Stress-Strain Behavior of Concrete in Compression

The behavior of concrete under compression and tension plays a vital role in accurately modeling its inelastic response. In finite element modeling, stress-strain relationships define the nonlinear characteristics of concrete, including the strain-softening effect in tension and the nonlinear stress-strain response in compression [25]. Stress-strain data are typically obtained from cube or cylinder tests; however, cylinder tests are considered more accurate for inelastic modeling. Analytically can be defined using expressions (1), (2), and (3), and Figure 3 [26]. In this study, the stress-strain behavior in compression, along with damage parameters, is calculated using Figure 3 and expressions (1), (2), and (3), and the results are presented in Figure 4, which presents the progression and intensity of damage based on the applied criteria.

$$\sigma = \sigma_{\text{cu}} \frac{k\eta - \eta^2}{1 + (k-2)\eta} \tag{1}$$

$$\eta = {}^{\varepsilon}/\varepsilon_{c1} \tag{2}$$

$$k = 1.05E_{c1}^{\epsilon_{c1}}/\sigma_{cu}$$
 (3)

Where, σ is stress in the concrete at a given strain (ϵ), σ_{cu} is the ultimate compressive strength of concrete, k is a dimensionless parameter that depends on the properties of concrete, η is a dimensionless strain ratio, ϵ is the strain in the concrete at the given point, ϵ_{c1} is the strain corresponding to the peak stress (σ_{cu}) in the concrete, E_{c1} is the initial tangent modulus of elasticity of concrete.

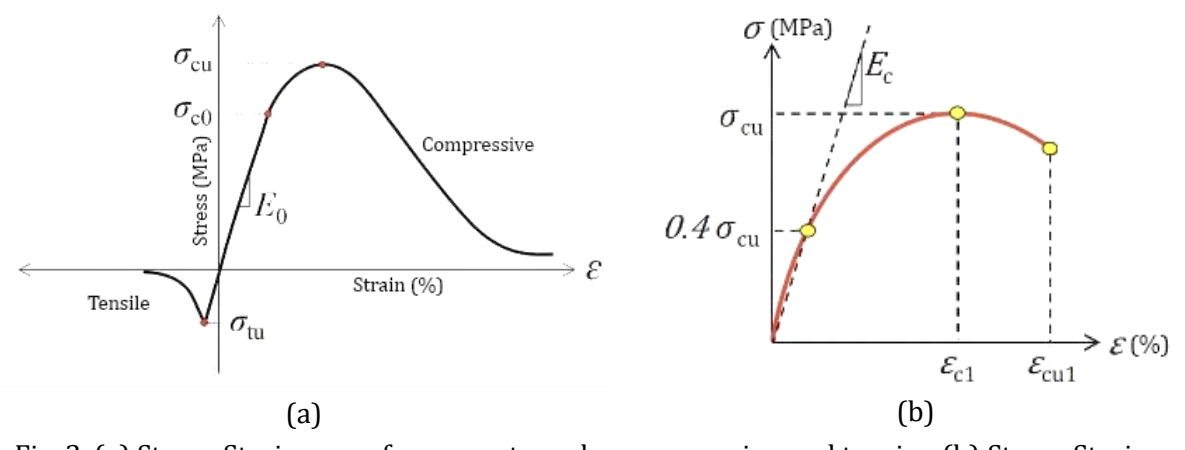


Fig. 3. (a) Stress-Strain curve for concrete under compression and tension (b) Stress-Strain Curve in compression [25]

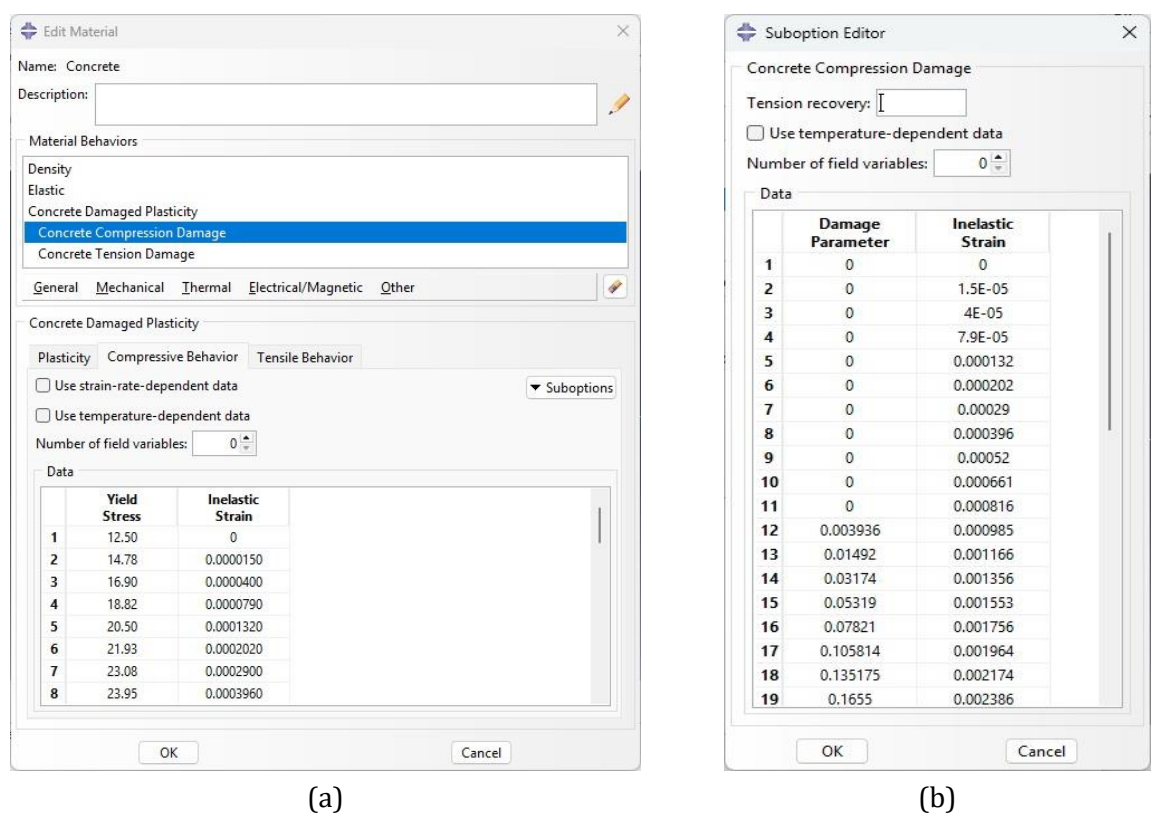


Fig. 4. (a) Stress-Strain behavior data in compression, (b) Damage parameters

4.1.2 Stress-Strain Behavior of Concrete in Tension

In tension, concrete behaves in a brittle way. Therefore, the softening behavior of concrete in tension can be modeled numerically. Typically, a linear, bilinear, or exponential softening law is used in numerical simulations. The softening behavior of concrete in tension is illustrated in Figure 5. In this study, the softening behavior data along with the damage parameters are calculated using the exponential softening law, based on Figure 5(c) and expressions (4) and (5). The estimated data are displayed in Figure 6 [25, 26].

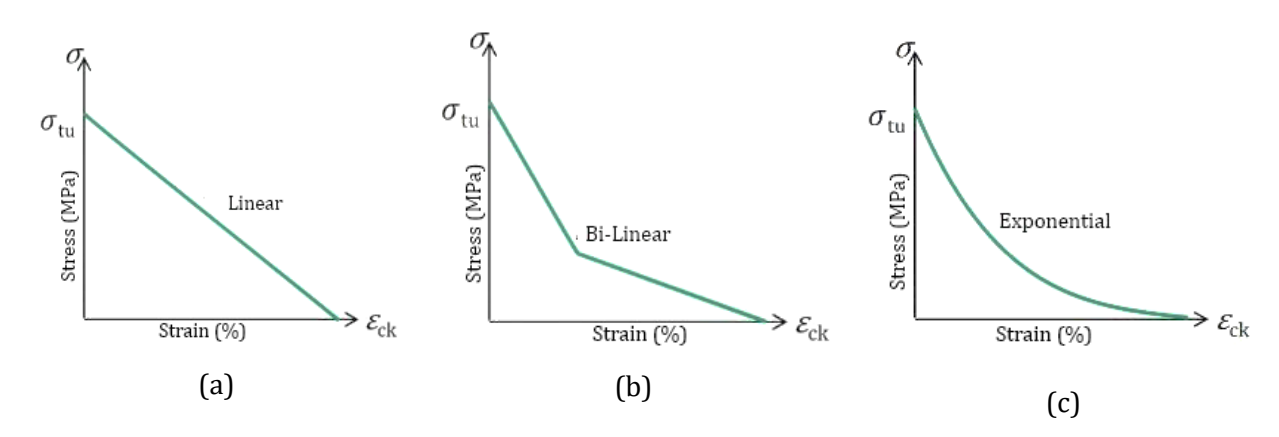


Fig. 5. (a), (b), and (c) Stress-strain curves illustrating the tensile softening behavior of concrete in the inelastic or plastic state

$$\sigma/f_t = \{1 + (c_1 \frac{w}{w_c})^3\} exp\left(-c_2 \frac{w}{w_c}\right) - \frac{w}{w_c}(1 + c_1^3) exp\left(-c_2\right)$$
(4)

$$d = 1 - \frac{\sigma}{E_0 \cdot \varepsilon} \tag{5}$$

Where, σ is the relative stress, f_t is the mean value of tensile strength, c_1 and c_2 represent constants, w is the crack opening, w_c is the critical crack opening, d indicates damage parameter, E_0 is the initial (undamaged) Young's modulus.

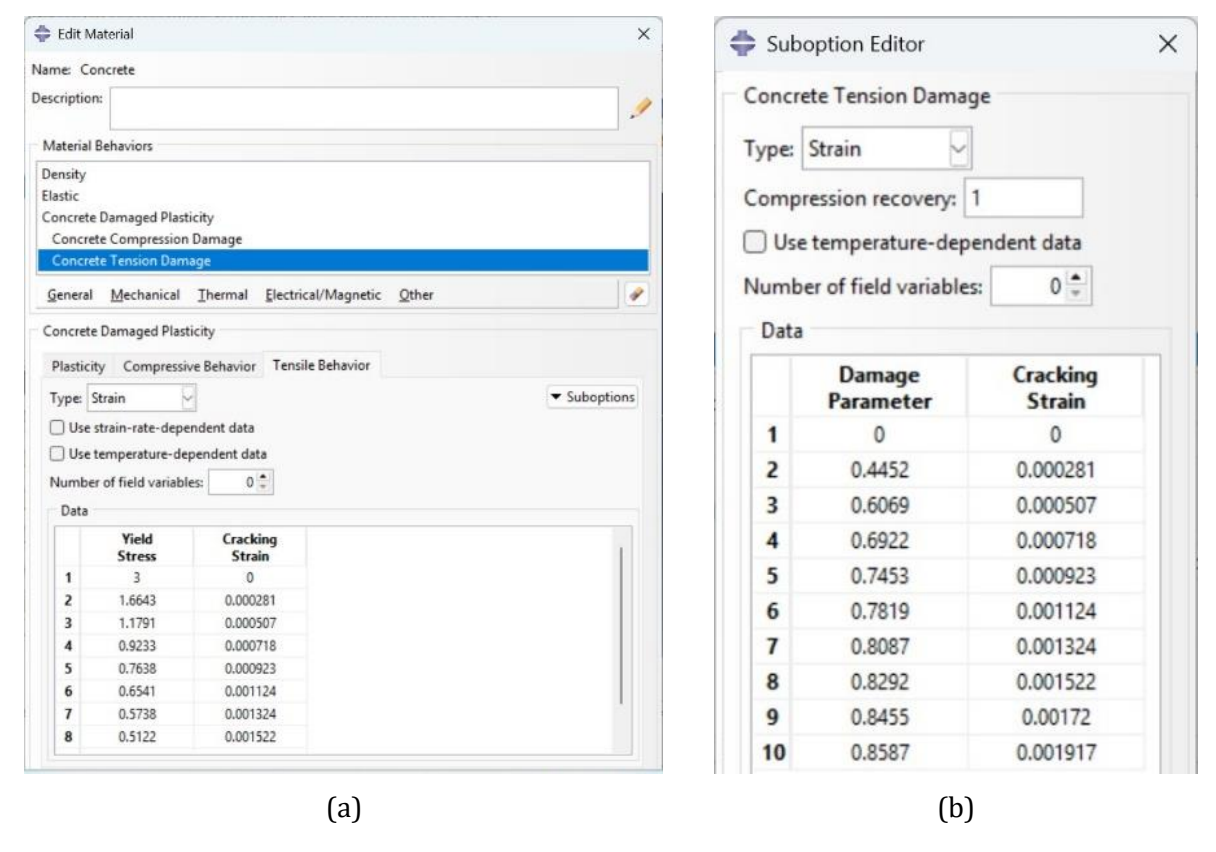


Fig. 6. (a) Stress-Strain behavior data in tension, (b) Damage parameters

4.1.3 Mesh Sensitivity in FEM

A mesh sensitivity analysis was conducted using element sizes of 40 mm, 30 mm, and 20 mm for the FEM model. The load deflection curve for the 20 mm mesh closely matched the experimental data, accurately reflecting both the initial stiffness and post-cracking behavior. The convergence of results between the 30 mm and 20 mm confirmed that the 20 mm mesh offers a good balance between computational efficiency and accuracy, and was therefore selected for the study. The results of the mesh sensitivity analysis are presented in Figure 7, which compares the load deflection response of the FEM model at different element sizes against the experimental results.

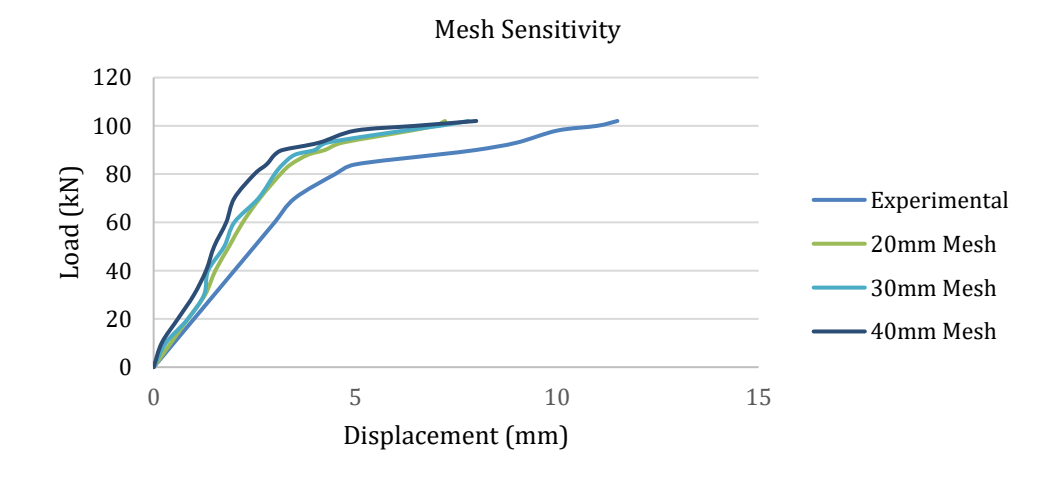


Fig. 7. Mesh sensitivity in FEM

Figure 7 demonstrates that the model's response is very sensitive to coarse meshes, but converges at 20 mm. The close alignment of the 20 mm mesh result with the experimental data confirms its suitability for capturing the beam's inelastic behavior.

4.2 Applied Element Modeling

The AEM is a computational method used to simulate structural performance, from elastic response to total collapse, by modeling structures as a combination of discrete elements. AEM discretizes a structure into small rigid elements connected by nonlinear spring interfaces. These springs represent normal and shear behavior, allowing the simulation of cracking, yielding, separation, and collision [27].

In this study, the ELS (Extreme Loading for Structures) program is used to model the inelastic behavior of an RC beam in terms of deflection, crack patterns, load-displacement curve, elastic with plastic moments, and failure type of the reinforced beam. AEM is chosen because of its ability to precisely model fracture propagation, excessive distortions, and gradual failure processes, which are vital for evaluating the performance of reinforced concrete elements [11]. The following formulas, (6) and (7), indicate the interface rigidity in transverse and longitudinal directions of the interfacing components.

$$K_n = \frac{E * d * T}{a} \tag{6}$$

$$\mathbf{K}_{\mathbf{s}} = \frac{\mathbf{G} \cdot \mathbf{d} \cdot \mathbf{T}}{2} \tag{7}$$

Where K_n and K_s are the orthogonal and transverse stiffnesses, T represents the thickness of the component, d indicates the distance among springs, a represents the length of the typical area, E and G denote Young's and shear modulus of the bonded materials, respectively. Figure 8 describes the modeling and configuration of the matrix springs using AEM [6].

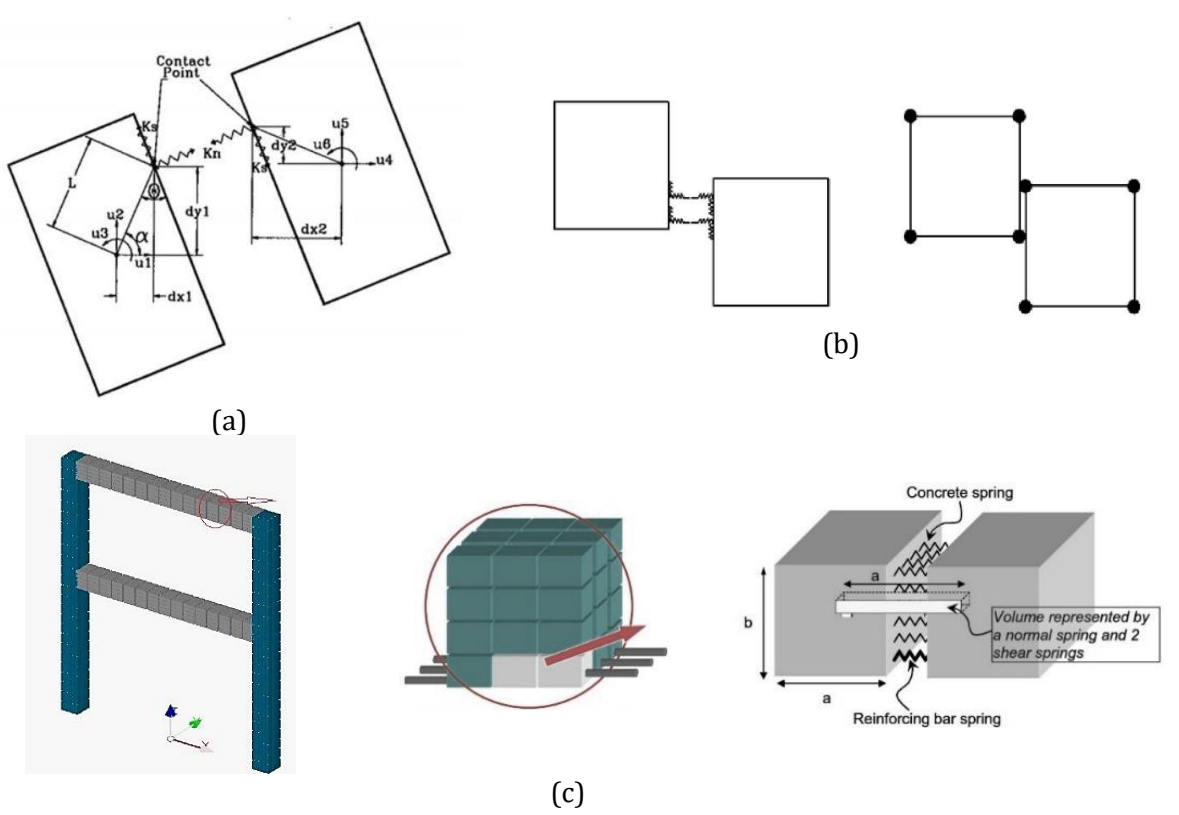


Fig. 8. (a) Contact point between two elements, (b) Element connectivity in AEM vs FEM, (c) Modeling of structure in AEM [6]

The beam was modeled as simply supported, replicating the experimental setup with pinned and roller supports at both ends to permit rotation while avoiding vertical translation. The beam geometry was based on Figure 2, while the material properties, including concrete compressive strength, tensile strength, and modulus of elasticity, were sourced from Table 2. Figure 9 presents the RC beam geometry and boundary conditions modeled in the ELS program. Unlike traditional FEM meshing, AEM divides the structure into discrete elements based on user-defined divisions in three directions (length, height, and width). A non-uniform mesh was applied with approximate element sizes of 20.20 mm, 11.90 mm, and 13.64 mm in the x, y, and z directions, respectively. For consistency in the comparative analysis, the AEM model was discretized using an element size of 20 mm along the longitudinal (x) axis, matching the mesh size used in the FEM model. The interface spring stiffnesses were calculated based on the provided formulas (6) and (7), which represent the shear and normal rigidities of the interfaces, respectively. Typical parameters used in the AEM model are summarized in Table 4 [28].

Table 4	Parameter	definitions	in AFM
I abic T.	1 ai aiiictei	ucililituolis	$\Pi \Pi \Pi \Pi \Pi \Pi \Pi$

Parameters	Symbol	Value	Unit	Description
Young's Modulus	Е	25000	MPa	Stiffness of material in the axial (normal) direction.
Shear Modulus	G	10416.66	MPa	Stiffness of material in shear direction.
Element Thickness	Т	1.515	mm	Thickness of 2D element, for 3D elements, this is replaced by element depth/volume.
Spring Spacing	d_x , d_y , d_z	20.2, 11.9, 13.64	mm	Distance between adjacent springs along the interface between two elements.
Area of Influence	ax, ay, az	162.3, 275.5, 240.3	mm²	Area associated with each spring (related to d and T).
Number of Elements (x, y, z)	N _x , N _y , N _z	99, 21, 11	-	Mesh discretization of the beam in three directions (x, y, z).
Normal Spring Stiffness (X, Y, Z, directions)	Kn	200.9, 578.7, 440.5	kN/mm	Stiffness against axial deformation
Shear Spring Stiffness (X, Y, Z, directions)	Ks	83.7, 241.1, 183.5	kN/mm	Stiffness against shear deformation
Total Number of Elements		22869		Total elements in model.

The geometry and boundary condition setup for the AEM analysis in ELS is presented in Figure 9. The model accurately represents the simply supported constraints and the application of the point load at mid-span, as per the experimental setup.

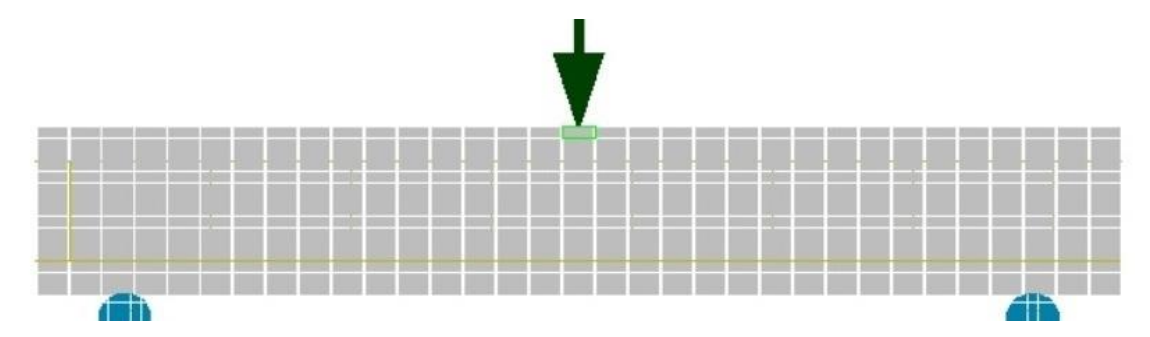


Fig. 9. RC beam geometry and boundary setup as modeled in ELS.

4.2.1 Mesh Sensitivity in AEM

Choosing the right mesh density is crucial for achieving results that are independent of discretization. The mesh size for the AEM model in this paper was based on the comprehensive

sensitivity analysis conducted by Alanani M. et al. [29], which examined the convergence of the ELS model for the RC beam. In this model, this led to a total of 22,869 elements, a number that aligns well with the stable, converged regime conducted in their sensitivity analysis. Figure 10, recreated based on the data from Alanani M. et al., shows the convergence criteria for the ELS model of RC beam, guiding the mesh choice in this study.

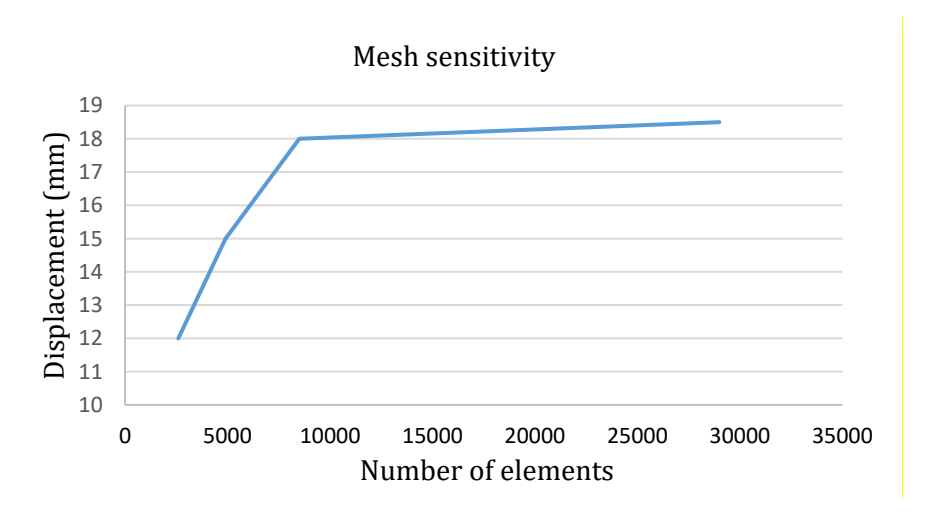


Fig. 10. Mesh sensitivity in AEM

Figure 10. Mesh sensitivity analysis for the AEM model. Beam displacement stabilizes once the total number of elements exceeds 10,000. The model in this study, with 22,869 elements, is well within this established convergence range.

5. Results and Discussions

5.1 Critical Load with Failure Mode

The cracking load marks the start of tensile fracture in the concrete section, denoting the transition from elastic to inelastic behavior in RC beams. In this paper, the average of the two independent experimental trials displayed a critical load of 43 kN, while the FEM and AEM produced cracking loads of 41 kN and 42 kN, respectively. The small variation (less than 6%) among the three methods demonstrates strong alignment in modeling the primary elastic behavior. This alignment suggests that both FEM and AEM simulations accurately represent the early-stage flexural behavior, including microcrack development and stress redistribution, consistent with Kwak and Kim's findings, who highlighted FEM's capability in the elastic zone [30].

Concerning the ultimate load in the plastic zone, the average of the two independent experimental trials' value was 103 kN. In comparison, FEM and AEM recorded 98 kN and 101 kN, respectively. The AEM results showed closer agreement with the experimental data, with a variation of 1.94%, compared to 4.8% for FEM. This indicates AEM's improved ability to model nonlinear performance beyond cracking and gradual failure, an ability assisted by Salem HM, et al. [31], who verified AEM's validity for RC structures under extreme loading conditions.

The failure mode was observed across all three models, two independent experimental trials, FEM, and AEM. All models experienced only pure flexure, with no signs of shear or torsional failure. This result highlights that the geometric configuration and loading setup of the beam accurately induced a bending-controlled response, which was closely captured by both numerical simulations. The consistency in the failure mode further confirms the accuracy of AEM in simulating real-world structural behavior, particularly under inelastic conditions, as noted in earlier investigations [32].

These findings highlight that both AEM and FEM can accurately model inelastic performance in structural elements with precision in RC beams. AEM shows slightly closer alignment with experimental data, especially in the inelastic region. This strengthens its structural compatibility for severe damage and collapse analysis in RC structures. The critical loads related to the failure modes are shown in Table 5 below.

Table 5. Critical load with Failure mode

Method	Cracking load (kN) in elastic zone	Ultimate load (kN) in plastic zone	Mode of Failure
Experimental (Trial_1-Trial_2)	(42-44)	(102-105)	Pure Flexure
FEM	41	98	Pure Flexure
AEM	42	101	Pure Flexure
Error AEM-FEM	2.33%-4.65%	1.94%-4.8%	N/A

5.2 Deflection

The load deflection behavior of the RC beam was studied under displacement-controlled loading conditions using FEM and AEM simulations. The load deflection behavior illustrated in Figure 11, observed from the numerical simulations, was correlated with the two independent experimental trials' results to validate the accuracy and reliability of the FEM and AEM numerical methods. The average data of the two experimental trials highlighted a gradual increase in deflection as the applied load increased, reaching a maximum deflection of 12 mm at a load of 103 kN. Both FEM and AEM models displayed similar responses, with deflections increasing as the load increases, though there is a marginal variation between the numerical models and the experimental data. During initial loading stages (10 kN to 50 kN), the FEM deflections are generally slightly less than the experimental results, with variations from 0.1 mm to 0.6 mm. This performance continues for the AEM model, which highlights deflections marginally higher than the FEM model; however, they remain close to the data from the two experimental trials.

As the load increases above 60 kN, both FEM and AEM simulations show a gradual rise in deflection, with the AEM model offering a minor improvement over FEM in terms of prediction reliability. As an illustration, at 70 kN, the AEM measures a deflection of 3.1 mm; whereas, the FEM shows 2.6 mm, which aligns with the average deflection of two experimental trials at 3.9 mm. The difference decreases at higher loads, and at 103 kN, the FEM predicts 7.2 mm deflection, while the AEM predicts 8.5 mm, compared to the average of the two experimental trials' outcomes of 12 mm. The model's accuracy was assessed using the Root Mean Square Error (RMSE) of deflection predictions at common load levels. RMSE values of 2.6 mm for FEM and 1.9 mm for AEM indicate that both numerical models capture the experimental deflection behavior with good accuracy.

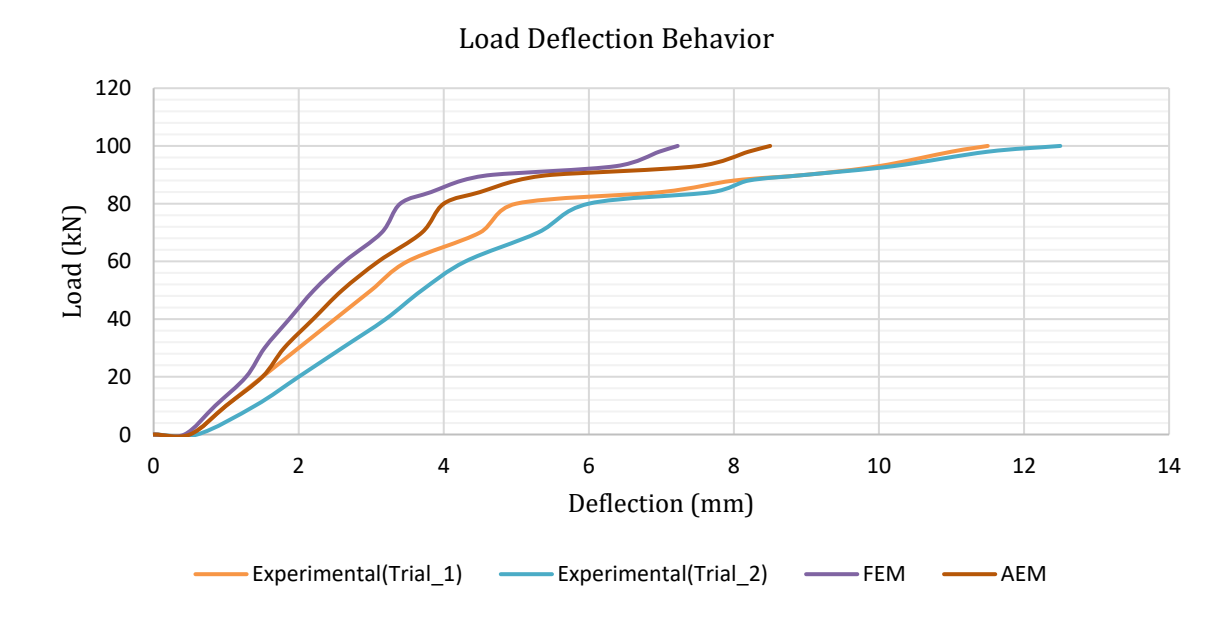


Fig. 11. Load deflection behavior

5.3 Critical Elastic and Plastic Moments

The numerical simulation was carried out using both the FEM and AEM, demonstrating consistent results in the elastic stage, where both methods indicated a critical moment value of 23 kN-m. This agreement verifies the reliability of both numerical modeling approaches in simulating the initial linear behavior of the RC beam under the applied loads. In contrast, during the plastic step, a slight difference was observed: the AEM estimated a plastic moment strength of 50 kN- m, while FEM indicated a slightly higher value of 53 kN-m. The 5.6% lower plastic moment in AEM arises from its explicit modeling of discrete fracture and post-yield redistribution, unlike FEM's smeared crack approach. FEM's higher estimate of the plastic moment capacity comes from continuum approximations that do not adequately resolve localized damage.

Similar patterns have been examined in previous studies, showing the effectiveness of AEM and FEM in capturing progressive damage and post-cracking behavior in RC structures [33, 34]. A closer match of AEM results with experimental data in the plastic domain, compared to traditional numerical modeling with FEM, was reported in a previous study by Mahrous et al. [35]. Additionally, earlier research has also highlighted that advanced continuum and discrete-based numerical models, like AEM, can illustrate the complex mechanisms and failure progression in RC members under different loading conditions [36, 37]. The critical elastic and plastic moments of the ultimate outcomes observed from both AEM and FEM numerical simulations are summarized in Figure 12, clearly illustrating the transition from elastic to plastic behavior and visualizing the consistency and relative reliability of both numerical methods in presenting the structural responses under increasing load conditions.

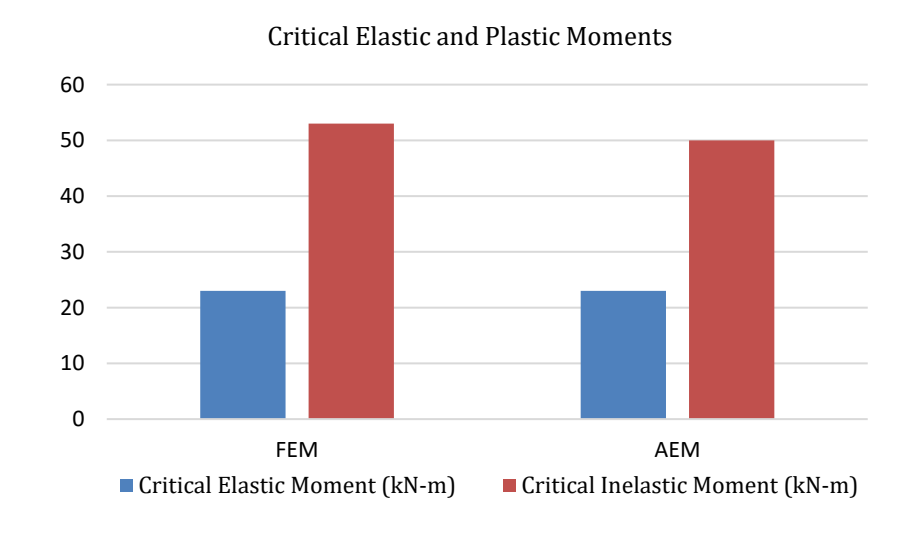


Fig. 12. Critical elastic and plastic moments

5.4 Crack Patterns

The crack patterns and deflected shapes observed from the experimental investigation, FEM, and AEM numerical simulation results are highlighted to evaluate the reliability of these methods, particularly with the AEM approach in presenting the inelastic behavior of the RC beam.

5.4.1 Experimental Results

The experimental crack patterns, as described in the literature, are shown in Figure 13 and present both the crack propagation and the related deflected shape of the RC beam under increased load [12]. These results provide a detailed view of the beam's failure mode and function as a benchmark for supporting numerical models. The failure mechanism of the FEM model is validated by analyzing its internal state at ultimate load. The damage progression is examined in Figure 14, while the related stress distribution is confirmed in Figure 15.



Fig. 13. Crack patterns and deflected shape [12]

5.4.2 FEM Results

5.4.2.1 Crack Pattern and Damage Evolution

The damage contours at ultimate load are presented in Figure 14. The tensile damage (DAMAGET) in Figure 14(a) reveals the pattern of flexural cracking, with values approaching 1.0 at the beam's bottom mid-span, indicating the formation of the primary plastic hinge. This is complemented by the compressive damage (DAMAGEC) in Figure 14(b), which shows concrete crushing at the top compression zone, completing the picture of a typical flexural failure mechanism.

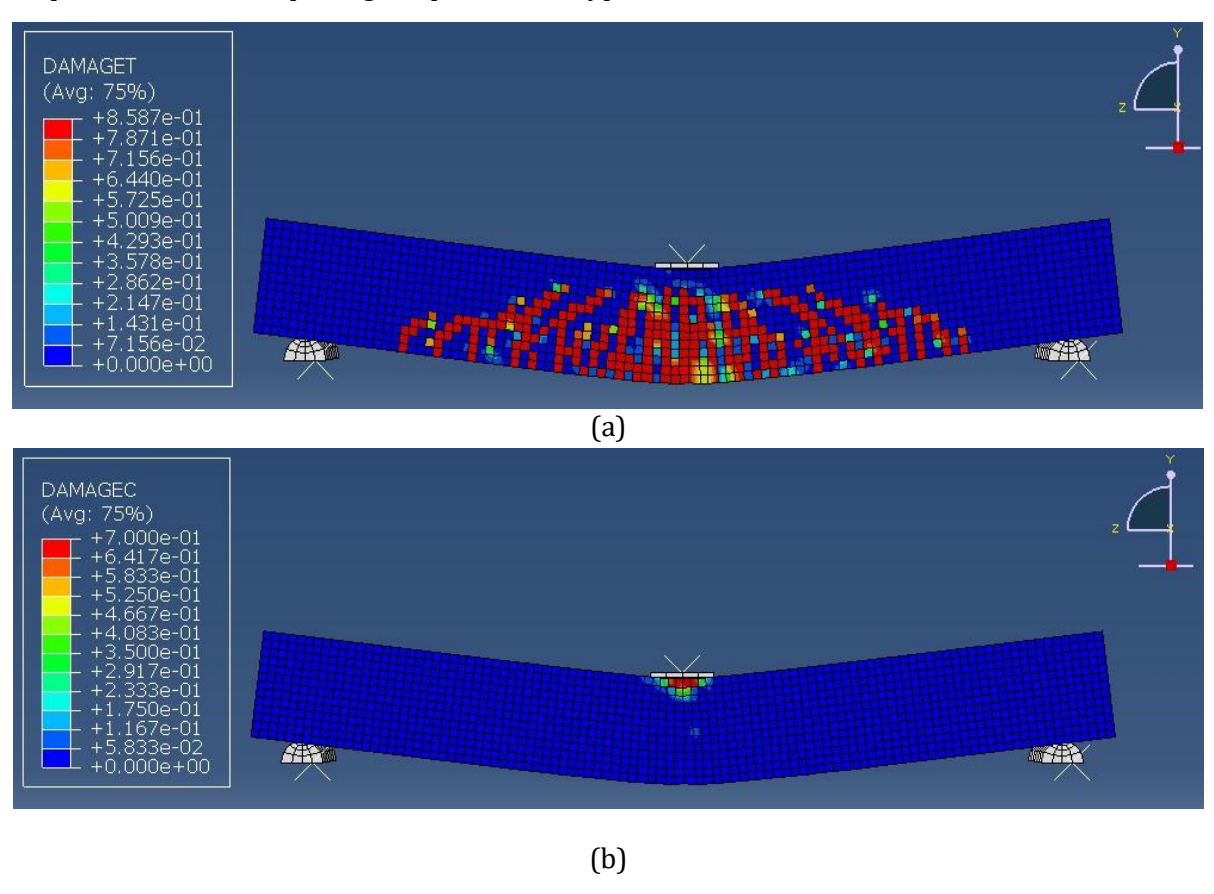
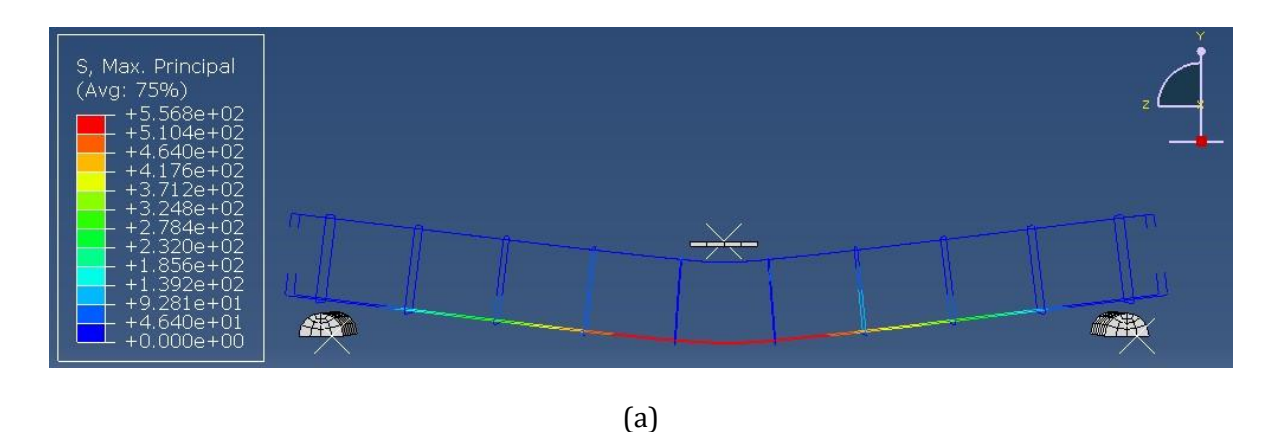


Fig. 14. (a) DAMAGET observed from FEM, deformation scale factor (5) and (b) DAMAGEC observed from FEM, deformation scale factor (5)

5.4.2.2 Stress Distribution

The stress contours showing the underlying force data are presented in Figure 15. The maximum principal stress (S, Max Principal) in the reinforcement, shown in Figure 15 (a), highlights the high tensile zones that led to the cracks. Additionally, the von Mises stress (S, Mises) in the reinforcement, shown in Figure 15(b), verifies that the steel has yielded, providing clear evidence of a ductile flexural failure mode and confirming the model's accuracy. Together, these contour

plots provide a comprehensive validation of the FEM model. The consistent match between the damage patterns, stress distributions, and experimental results confirms the model's accuracy in simulating the inelastic behavior and failure mechanism of the RC beam.



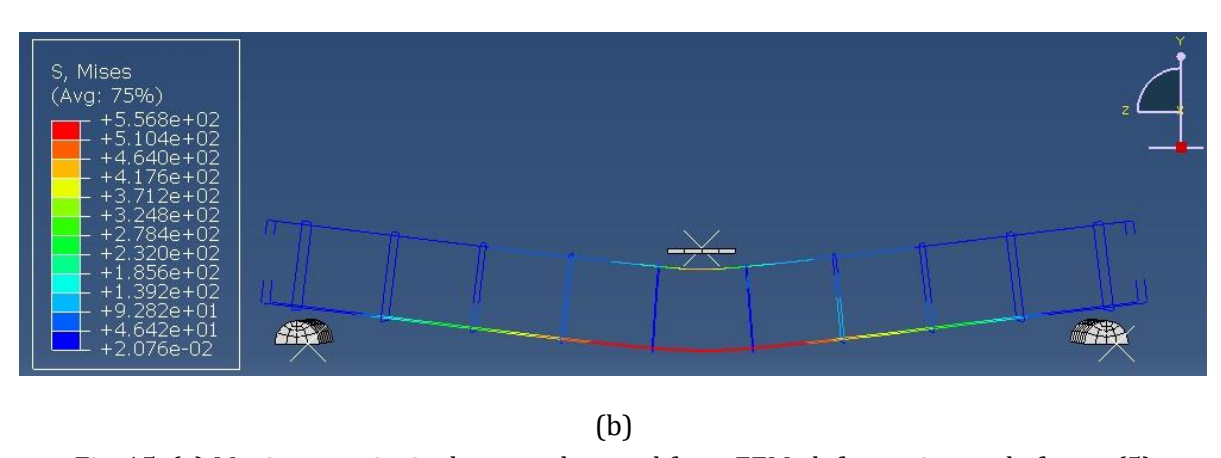


Fig. 15. (a) Maximum principal stress observed from FEM, deformation scale factor (5) (b) Maximum von Mises stress observed from FEM, deformation scale factor (5)

5.4.3 AEM Results

The AEM analysis results illustrate both crack patterns and deflected shapes simultaneously, accurately matching the experimental observations. Compared to FEM, AEM does not require detailed, predefined material properties for fracture development, as the numerical approach automatically allows cracking and crack propagation during the analysis, optimizing the modeling procedure while preserving accuracy [10]. The crack patterns and deflected shape of the simulated beam using ELS are shown in Figure 16.



Fig. 16. Crack patterns and deflected shape observed from AEM

The assessment among numerical methods demonstrates that AEM not only accurately captures crack initiation and expansion but also effectively highlights the overall load-deflection behavior. These results match with earlier investigations, which similarly confirmed the strengths of AEM in

presenting both crack patterns and displacement behavior compared to experimental outcomes [38, 39].

The correlation between crack patterns and deflected shapes from experimental results, FEM, and AEM demonstrates the reliability of numerical methods in analyzing the inelastic behavior of RC beams. Literary experimental observations showed both crack patterns and load deflection behavior, serving as a benchmark for verification. In FEM simulation using Abaqus software, the crack patterns primarily indicated pure flexural performance, which fully aligns with experimental observations.

5.5 Summary of the Results

To provide a clear overall assessment of the predictive ability of the numerical models, Table 6 summarizes the key results from the experimental program, the FEM, and the AEM. The table also reports the absolute and percentage errors of the numerical results compared to the experimental data. As shown, both FEM and AEM results align well with the experiments, with percentage errors typically below 6% across all key parameters.

Table 6. Summary of the results

Description	Experimental Trial_1	Experimental Trial_2	FEM	Abs. Error (FEM)	% Error (FEM)	AEM	Abs. Error (AEM)	% Error (AEM)
Cracking load (kN) in elastic zone	42	44	41	2.00	4.65%	42	1.00	2.33%
Ultimate load (kN) in plastic zone	102	105	98	5.50	5.31%	101	2.50	2.42%
Global deflection RMSE (mm)	-	-	2.6	-	-	1.9	-	-
Elastic moment (kN-m)	-	-	23	-	-	23	-	-
Plastic moment (kN-m)	-	-	53	-	-	50	-	-
Mode of failure	Pure Flexure	Pure Flexure	Pure Flexure	-	-	Pure Flexure	-	-

Overall, both numerical models closely matched the experimental load-deflection response and crack patterns, particularly in the elastic region. The FEM model provides reasonable predictions of the initial stiffness and yield load but requires careful calibration of parameters, such as the concrete damage plasticity, to achieve stable post-failure results. These findings align with previous studies, confirming that both FEM and AEM are well-suited for modeling inelastic behavior.

6. Conclusion

6.1 Conclusion Based on AEM and FEM

This paper presents a comprehensive numerical study of the inelastic behavior and failure mechanisms of a reinforced concrete beam, employing both the AEM and FEM numerical methods. The key finding verifies that reinforced concrete beams have a significant capacity for inelastic deformation, clearly demonstrating their capacity to withstand loads up to twice their elastic serviceability limit before failure. This result provides accurate numerical validation for established experimental observations, strengthening our understanding of ductile structural behavior.

A key insight from this comparative analysis is the accurate simulation of failure modes. Both numerical models successfully captured the formation of a plastic hinge at the mid-span under

flexural loading, which was validated by experimental results. This failure was characterized by the yielding of the longitudinal tensile reinforcement, followed by concrete crushing in the compression zone at the mid-span, forming a plastic hinge. Furthermore, the deformation analysis validated both models, with close RMSE values of 2.6 mm (FEM) and 1.9 mm (AEM), confirming their accuracy in simulating overall structural response. While both methods reliably predicted deflection behavior, AEM's marginally lower error demonstrates its particular effectiveness in capturing the complete nonlinear path through collapse, whereas FEM remains a strong choice for general deformation analysis.

The evaluation of moment capacity revealed that both FEM and AEM produced identical results of 25 kN-m in the elastic stage, confirming their equivalent accuracy for linear analysis. In the plastic stage, however, a divergence was observed, with AEM predicting a plastic moment of 50 kN-m compared to 53 kN-m from FEM. While the absence of experimental data for direct validation precludes a definitive accuracy assessment, this discrepancy highlights a meaningful difference in how the methods model post-yield behavior and ultimate section capacity under inelastic conditions.

Qualitatively, both the AEM and FEM models successfully replicated the fundamental flexural crack pattern observed in the experimental benchmark, confirming their ability to capture the primary failure mechanism. For a more detailed quantitative analysis of the internal state, the FEM model provided comprehensive data, including stress contours (S, Mises; S, Max Principal) and damage metrics (DAMAGET, DAMAGEC), as requested during the review process. These detailed outputs from FEM offered valuable insight into the progression of tensile cracking and compressive crushing within the concrete continuum. While a direct, equally detailed comparison from AEM was not feasible due to software access constraints, the agreement in the global crack pattern between both methods and the experiment underscores that, while FEM offers superior detail for micro-level stress analysis, AEM remains highly effective for predicting the macro-level structural damage and collapse mode.

6.2 Limitations and Future Work

This study, while offering valuable insights into the inelastic response of under-reinforced RC beams simulated with AEM and FEM, has certain limitations that suggest directions for future research. The scope was intentionally limited to under-reinforced beam sections to concentrate on a specific ductile failure mechanism; consequently, the applicability findings to over-reinforced or balanced sections, which display significantly different brittle failures, remain an open question. Additionally, the study was limited to quasi-static, displacement-controlled loading conditions.

Building on the foundational mesh sensitivity analysis presented here, future work should include a more detailed parametric study. This should involve varying key parameters such as shear span to depth ratio, concrete strength, and especially the reinforcement ratio to systematically explore the performance of AEM and FEM across a wider range of designs. Additionally, it would be important to extend the comparison to cyclic and dynamic loading conditions to fully evaluate the methods' effectiveness for simulating seismic or impact scenarios.

References

- [1] Yön B, Dedeoğlu İÖ, Yetkin M, Erkek H, Calayır Y. Evaluation of the seismic response of reinforced concrete buildings in the light of lessons learned from the February 6, 2023, Kahramanmaraş, Türkiye earthquake sequences. Natural Hazards. 2025 Jan;121(1):873-909. https://doi.org/10.1007/s11069-024-06859-9
- [2] Meguro K, Tagel-Din HS. applied element method used for large displacement structural analysis. Journal of Natural Disaster Science. 2002 Jun 1;24(1):25-34. https://jsnds.org/jnds/24_1_3.pdf
- [3] Meguro K. Fracture Behavior Analysis of Structures Using A New Efficient and Simple Technique. Production Research: Bulletin of the Institute of Industrial Science, University of Tokyo, Journal of the Institute of Industrial Science, The University of Tokyo. 1997;49(11):577-80.
- [4] Meguro K, Tagel-Din H. Applied element simulation of RC structures under cyclic loading. Journal of Structural Engineering. 2001 Nov;127(11):1295-305. https://doi.org/10.1061/(ASCE)0733-9445(2001)127:11(1295)
- [5] Tagel-Din H, Rahman NA. The Applied Element Method: the ultimate analysis of progressive collapse. STRUCTURE magazine. 2006 Apr; 4:30-3.

- [6] Meguro K, Tagel-Din H. Applied element method for structural analysis theory and application for linear materials. Doboku Gakkai Ronbunshu. 2000 Apr 21;2000(647):31-45. https://doi.org/10.2208/jscej.2000.647_31
- [7] Alanani M, Ehab M, Salem H. Progressive collapse assessment of precast prestressed reinforced concrete beams using applied element method. Case Studies in Construction Materials. 2020 Dec 1;13:e00457. https://doi.org/10.1016/j.cscm.2020.e00457
- [8] Botez MI, Bredean LU, Ioani AM. Numerical methods in progressive collapse assessment of RC framed structures: FEM vs. AEM. Proc. 5th Int. Congr. Comput. Mech. Simul., Research Publishing Services, Singapore. 2014 Dec 10:1865-73. https://doi:10.3850/978-981-09-1139-3_213
- [9] Tagel-Din H, Meguro K. Applied element simulation for collapse analysis of structures. Bulletin of Earthquake Resistant Structure Research Center. 1999 Mar;32(3):113-23.
- [10] Shakeri A, Bargi K. Use of applied element method for structural analysis. KSCE Journal of Civil Engineering. 2015 Jul 1;19(5):1375-84. https://doi:10.1007/s12205-015-0625-4
- [11] Meguro K, Tagel-Din H. A new efficient technique for fracture analysis of structures. Bulletin of Earthquake Resistant Structure Research Center, IIS, Univ. of Tokyo. 1997 Mar; 30:103-16.
- [12] Azeez MR, Bhojaraj M, Ravikumar M, Bhanulatha GN. Experimental Study on Plastic Failure of Reinforced Concrete Beams. International Journal of Applied Engineering Research. 2018;13(7):38-41.
- [13] Ayoub A, Filippou FC. Nonlinear finite-element analysis of RC shear panels and walls. Journal of Structural Engineering. 1998 Mar;124(3):298-308.
- [14] Earij A, Alfano G, Cashell K, Zhou X. Nonlinear three–dimensional finite-element–element modelling of reinforced–concrete beams: Computational challenges and experimental validation. Engineering Failure Analysis. 2017 Dec 1;82:92-115, https://doi:10.1016/j.engfailanal.2017.08.025
- [15] Halahla A. Study the behavior of reinforced concrete beam using finite element analysis. In Proceedings of the 3rd World Congress on Civil, Structural, and Environmental Engineering 2018 Apr (Vol. 10). https://DOI:10.11159/icsenm18.103
- [16] Demir A, Ozturk H, Dok G. 3D numerical modeling of RC deep beam behavior by nonlinear finite element analysis. Disaster Science and Engineering. 2016 Apr;2(1):13-8.
- [17] Castaldo P, Gino D, Bertagnoli G, Mancini G. Partial safety factor for resistance model uncertainties in 2D non-linear finite element analysis of reinforced concrete structures. Engineering structures. 2018 Dec 1;176:746-62. https://doi.org/10.1016/j.engstruct.2018.09.041
- [18] Applied Science International. Extreme Loading for Structures (ELS). Version 8.0. Durham, NC, USA: Applied Science International, LLC.; 2021.
- [19] Al-Khafaji FF. Enhancing the performance of cold bitumen emulsion mixtures with coir and glass fibres: Experimental and numerical analysis. Research on Engineering Structures and Materials. 2025. http://dx.doi.org/10.17515/resm2025-786ma0327rs
- [20] Masne N, Pawar A. Experimental and numerical investigation of solid and hollow recycled aggregate concrete beams subjected to torsion. Research on Engineering Structures and Materials. 2024. http://dx.doi.org/10.17515/resm2024.457me0920rs
- [21] Hemamathi A, Sukumar B, Chantrakant RH. Numerical Analysis of RCC Beam Using ABAQUS. In IOP Conference Series: Earth and Environmental Science 2022 Oct 1 (Vol. 1084, No. 1, p. 012077). IOP Publishing. https://doi:10.1088/1755-1315/1084/1/012077
- [22] Dassault Systèmes. ABAQUS/CAE. Version 2022. Providence, RI, USA: Dassault Systèmes Simulia Corp.; 2022.
- [23] Raju MR. Analysis of RCC Beams using ABAQUS. International Journal of Innovations in Engineering and Technology (IJIET). Vol. 5. 2015 3 June: 2319 1058.
- [24] Fagerhøi S, Bergsbakken AK. Abaqus FEA with Concrete Damaged Plasticity and its feasibility in recreating laboratory experiments: A numerical analysis and sensitivity study (Master's thesis, OsloMet-Storbyuniversitetet). https://hdl.handle.net/11250/3101600
- [25] Lee J, Fenves GL. Plastic-damage model for cyclic loading of concrete structures. Journal of Engineering Mechanics. 1998 Aug;124(8):892-900. https://doi.org/10.1061/(ASCE)0733-9399(1998)124:8(892)
- [26] Hordijk DA. Tensile and tensile fatigue behaviour of concrete; experiments, modelling and analyses. Heron. 1992;37(1).
- [27] Tagel-Din H, Meguro K. Analysis of a small-scale RC building subjected to shaking table tests using Applied Element Method. In Proceedings of the 12th World Conference on Earthquake Engineering, New Zealand 2000 (pp. 1-8).
- [28] Tagel-Din H, Meguro K. Consideration of Poisson's ratio effect in structural analysis using elements with three degrees of freedom. Bull. of Earthquake Resistant Struct. Res. Ctr. 1998;31:41-50.
- [29] Alanani M, Ehab M, Salem H. Progressive collapse assessment of precast prestressed reinforced concrete beams using applied element method. Case Studies in Construction Materials. 2020 Dec 1;13:e00457. https://doi.org/10.1016/j.cscm.2020.e00457

- [30] Kwak HG, Kim SP. Nonlinear analysis of RC beams based on moment-curvature relation. Computers & structures. 2002 Mar 1;80(7-8):615-28. https://doi.org/10.1016/S0045-7949(02)00030-5
- [31] Salem HM, El-Fouly AK, Tagel-Din HS. Toward an economic design of reinforced concrete structures against progressive collapse. Engineering Structures. 2011 Dec 1;33(12):3341-50. https://doi.org/10.1016/j.engstruct.2011.06.020
- [32] Gohel V, Patel PV, Joshi D. Analysis of frame using applied element method (AEM). Procedia Engineering. 2013 Jan 1;51:176-83. https://doi:10.1016/j.proeng.2013.01.026
- [33] Galano S, Losanno D, Miluccio G, Parisi F. Multidimensional nonlinear numerical simulation of post-tensioned concrete girders with different prestressing levels. Structural Concrete. 2023 Dec;24(6):7021-42. https://doi:10.1002/suco.202300272
- [34] Hanganu AD, Onate E, Barbat AH. A finite element methodology for local/global damage evaluation in civil engineering structures. Computers & Structures. 2002 Aug 1;80(20-21):1667-87. https://doi.org/10.1016/S0045-7949(02)00012-3
- [35] Mahrous A, Ehab M, Salem H. Progressive collapse assessment of post-tensioned reinforced concrete flat slab structures using AEM. Engineering Failure Analysis. 2020 Jan 1;109:104278. https://doi.org/10.1016/j.engfailanal.2019.104278
- [36] Lourenço PB, Silva LC. Computational applications in masonry structures: from the meso-scale to the super-large/super-complex. International Journal for Multiscale Computational Engineering. 2020;18(1). https://doi:10.1615/Int]MultCompEng.2020030889
- [37] Eraky A, A Mustafa SA, Badawy M. Structural analysis using Applied Element Method: a review. The Egyptian International Journal of Engineering Sciences and Technology. 2021 Jun 1;34(1):16-27. https://dx.doi.org/10.21608/eijest.2021.56786.1043
- [38] Christy DL, Pillai TM, Nagarajan P, Manimaran L. Determination of Crack Pattern in Concrete Structures Using Applied Element Method. In Materials Science Forum 2019 Oct 30 (Vol. 969, pp. 303-308). Trans Tech Publications Ltd. https://doi.org/10.4028/www.scientific.net/MSF.969.303
- [39] Beshara FB, El-Mahdy OO, Mahmoud A, Abbass MA. Simulating of RC Frames under Progressive Collapse Using AEM. International Journal of Advanced Engineering and Business Sciences. 2023 Feb 1;4(1):110-38. https://doi:10.21608/IJAEBS.2023.164905.1043

Appendix: Data Tables Used in Numerical Analysis

		Parameters Used i	n AEM Mode	lling	
	Parameters	Symbol		Value	Unit
Y	oung's Modulus	Е	25000		MPa
:	Shear Modulus	G		10416.66	MPa
Ele	ement Thickness	T		1.515	mm
:	Spring Spacing	d_x , d_y , d_z	20	0.2, 11.9, 13.64	mm
A	rea of Influence	a_x , a_y , a_z	162	2.3, 275.5, 240.3	mm^2
Numbe	er of Elements (x, y, z)	N _x , N _y , N _z		99, 21, 11	-
	Spring Stiffness (X, Y, Z, directions)	Kn	200	0.9, 578.7, 440.5	kN/mm
Shear S	pring Stiffness (X, Y, Z, directions)	Ks	83.7, 241.1, 183.5		kN/mm
Total	Number of Elements		22869		
	Data for Concrete			Data for Steel	
M25	Density (Ton/mm ³)	2.4E-09	Fe500	Density (Ton/mm ³)	7.85E-09
Elastic	Young's Modulus (MPa)	25000	Elastic	Young's Modulus (MPa)	2x10 ⁵
	Poisson's Ratio	0.2		Poisson's Ratio	0.3
	_		Plastic	Yield Stress (MPa)	550
			Plas	Plastic Strain	0
Plastic 		Concrete damage			
Pla	Dilation Angle	Eccentricity	fb ₀ /fc _o	К	Viscosity parameter
	34	0.1	1.15	0.666	0.0001

Azizi and Yajdani / Research on Engineering Structures & Materials x(x) (xxxx) xx-xx

	Compressive	e Behavior		=	Ton	sile Behavior	
Inela	Inelastic Damage		Tensile Behavior				
Yield Stress (MPa)	Strain (%)	Parameter, d _c	Inelastic Behavior	Yield Stress (MPa)	Cracking Strain (%)	Damage Parameter, d _t	Cracking Strain (%)
12.50	0	0	0	3	0	0	0
14.78	0.0000150	0	1.50E-05	1.6643	0.00028	0.4452	0.000281
16.90	0.0000400	0	4.00E-05	1.1791	0.00051	0.6069	0.000507
18.82	0.0000790	0	7.90E-05	0.9233	0.00072	0.6922	0.000718
20.50	0.0001320	0	0.00013	0.7638	0.00092	0.7453	0.000923
21.93	0.0002020	0	0.0002	0.6541	0.00112	0.7819	0.001124
23.08	0.0002900	0	0.00029	0.5738	0.00132	0.8087	0.001324
23.95	0.0003960	0	0.0004	0.5122	0.00152	0.8292	0.001522
24.55	0.0005200	0	0.00052	0.4634	0.00172	0.8455	0.00172
24.89	0.0006610	0	0.00066	0.4237	0.00192	0.8587	0.001917
25.00	0.0008160	0	0.00082				
24.90	0.0009850	0.003936	0.00099				
24.63	0.0011660	0.01492	0.00117				
24.21	0.0013560	0.03174	0.00136				
23.67	0.0015530	0.05319	0.00155				
23.04	0.0017560	0.07821	0.00176				
22.35	0.0019640	0.105814	0.00196				
21.62	0.0021740	0.135175	0.00217				
20.86	0.0021710	0.1655	0.00217				
20.09	0.0025980	0.1964	0.0026				
19.31	0.0028110	0.2274	0.00281				
18.55	0.0030230	0.258	0.00302				
17.80	0.0032350	0.288	0.00302				
17.07	0.0032330	0.3172	0.00324				
	0.0034430						
16.36		0.3454	0.00365				
15.68	0.0038600	0.3727	0.00386				
15.03	0.0040650	0.3988	0.00407				
14.40	0.0042680	0.4238	0.00427				
13.81	0.0044690	0.4476	0.00447				
13.24	0.0046690	0.4704	0.00467				
12.70	0.0048660	0.492	0.00487				
12.18	0.0050620	0.5126	0.00506				
11.70	0.0052570	0.5321	0.00526				
11.23	0.0054490	0.5507	0.00545				
10.79	0.0056410	0.5683	0.00564				
10.37	0.0058300	0.585	0.00583				
10.00	0.0060100	0.6	0.00601				
9.60	0.0062060	0.6159	0.00621				
9.24	0.0063920	0.6302	0.00639				
8.91	0.0065760	0.6437	0.00658				
8.58	0.0067600	0.6566	0.00676				
8.28 7.99	0.0069420 0.0071240	0.6688 0.68053	0.00694 0.00712				
7.71	0.0073040	0.6915	0.00712				
7.50	0.0074480	0.7	0.00745				